

## Submicron-Scale Surface Roughening Induced by Ion Bombardment

Elliott A. Eklund, R. Bruinsma, and J. Rudnick

*Department of Physics, University of California, Los Angeles, California 90024-1547*

R. Stanley Williams

*Department of Chemistry and Biochemistry, University of California, Los Angeles, California 90024-1569*

(Received 4 January 1991)

The scanning tunneling microscope (STM) was used to quantitatively investigate nonequilibrium surfaces of graphite roughened by sputter etching with 5-keV Ar ions. The resulting surface morphology depended strongly on the ion flux and fluence, as well as the sample temperature. The height-correlation functions of the roughened surfaces were calculated directly from the STM topographs and compared to linear-response theory and scaling analyses for the propagation of growing fronts. The surfaces developed correlated structures characterized by a length that diverged with increasing ion fluence.

PACS numbers: 68.55.Jk, 79.20.Rf, 81.15.Cd

One of the fundamental problems in materials science is to understand the effects of particle radiation on solid surfaces [1-3]. For example, the properties of sputter-deposited thin films depend sensitively on the surface morphology that is in turn determined by the sputter-growth process [4]. A similar situation exists for ion-beam sputter etching, a widely used technique in surface science and microelectronics, which also produces non-equilibrium surfaces with topography that depends on the sputtering conditions.

In general, surfaces exposed to high levels of particle radiation develop characteristic morphologies. On the macroscopic level (i.e., length scales larger than 1  $\mu\text{m}$ ), the effects of particle radiation are well understood. Ion bombardment erodes prominent surface features such as edges, corners, or peaks because exposed features receive a larger amount of flux. This radiation erosion is further enhanced by surface diffusion and evaporation and recondensation. In the continuum description of this process, one either assumes that the local erosion rates are proportional to the local incoming flux, or one uses the Huygens principle [5]. Numerical studies of macroscopic evolution have obtained results that compare favorably with experiments [6,7].

At the submicron level, our understanding is much less complete [8]. Electron-microscope studies of sputter-etched samples indicate that particle radiation will *roughen* a surface rather than smooth it, and prominent conelike features have been reported [9,10]. Both analytical studies and numerical simulations [11,12] indicate that the inclusion of shot noise in continuum theories produces rough nonequilibrium surfaces. The roughening is characterized by a correlation length  $\xi(t)$  that diverges with etching time  $t$ . Until now, however, there has been little experimental confirmation of this description.

In this Letter, we report on our use of a scanning tunneling microscope (STM) [13] to examine the surface topography of graphite after sputter etching. The STM offers unique opportunities for the study of radiation ero-

sion because it can *quantitatively* measure the height profile  $h(\mathbf{r})$  of a surface with very high resolution over a wide range of length scales. This allows us to calculate the height-correlation function [14]  $\langle |h(\mathbf{q})|^2 \rangle$ , defined as

$$\langle |h(\mathbf{q})|^2 \rangle = \frac{1}{\text{area}} \int \frac{d^2r}{(2\pi)^2} e^{i\mathbf{q}\cdot\mathbf{r}} \langle [h(0) - h(\mathbf{r})]^2 \rangle_t, \quad (1)$$

with  $\langle \dots \rangle_t$  indicating a sample average after  $t$  seconds of exposure. In other roughening problems, e.g., thermal roughening, the corresponding correlation function was a good measure of the overall surface geometry [15]. Because of loss of phase information in the height-correlation function, however, it is less sensitive to uncorrelated—but prominent—surface features, which are much more easily visible in the real-space STM topographs.

The surface chosen for this investigation was the (0001) face of highly oriented pyrolytic graphite (HOPG), which is easily cleaved to produce large, atomically flat regions [13]. This cleaved surface is inert when exposed to air and is easily imaged with the STM. In addition, graphite has a rigid lattice, as seen by its melting temperature of  $\sim 3800^\circ\text{C}$ . This indicates that surface diffusion effects should be small at room temperature and that topographical features produced by the bombardment are “frozen in” and can be observed with the STM long after the sputtering has taken place.

The graphite samples were cleaved to expose fresh surfaces and were then examined with the STM before sputter etching. The microscope was operated at atmospheric pressure in the constant-current mode, with a tunnel current of 0.5 nA and a sample-to-tip bias of  $-100$  mV. No filtering or data enhancement was necessary because of the especially high stability of our STM and its insensitivity to vibrational and electrical noise as well as thermal drift. Images taken at the largest scan size ( $2400 \text{ \AA} \times 2400 \text{ \AA}$ ) show large, atomically flat areas over many thousands of square  $\text{\AA}$ , while at higher magnifications (e.g.,  $25 \text{ \AA} \times 25 \text{ \AA}$ ) the familiar atomic scale

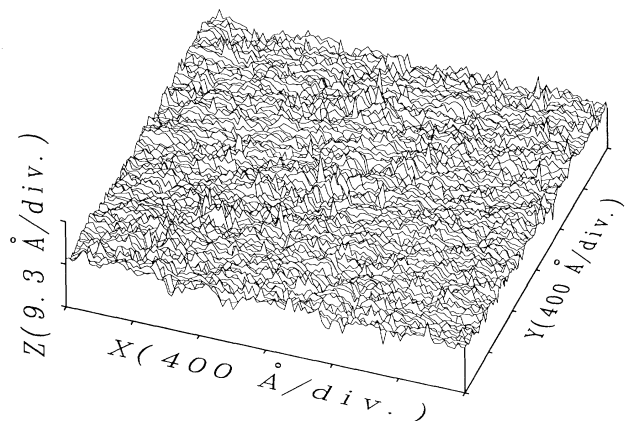


FIG. 1. Constant-current STM topograph of a graphite surface after sputtering with a flux  $J$  of  $6.9 \times 10^{13}$  ions/cm<sup>2</sup>sec and an ion fluence  $Q$  of  $10^{16}$  ions/cm<sup>2</sup> at room temperature. The  $X$  and  $Y$  dimensions are 2400 Å and the total  $Z$  dimension is 18.6 Å.

features of clean graphite were easily observed [13].

After stable images of clean graphite were obtained at both high and low magnifications, the samples were transferred from the STM to the sample treatment chamber of a KRATOS XSAM-800 surface analytical system. The graphite surfaces were sputter etched with a beam of 5-keV Ar<sup>+</sup> ions, rastered over a 9-mm<sup>2</sup> area on the sample and incident at an angle of 60° to the surface normal. The ion flux incident on the sample was determined by using an electrometer to measure the beam current. A small positive bias (45 V) was applied to the sample to suppress secondary electron emission. The experimental parameters that were varied in this study were the ion flux  $J$ , the fluence  $Q = Jt$ , and the substrate temperature  $T$ .

This Letter highlights the results obtained from over 1000 STM topographs collected from more than fifteen bombarded samples. The two fluxes reported here are  $6.9 \times 10^{13}$  ions/cm<sup>2</sup>sec and  $3.5 \times 10^{14}$  ions/cm<sup>2</sup>sec. By varying the time of exposure to the ion beam, the total fluences obtained were  $10^{16}$ ,  $10^{17}$ , and  $10^{18}$  ions/cm<sup>2</sup>. In addition to the ambient-temperature experiments, etching was also performed at surface temperatures of approximately 600 and 900 K for a flux of  $3.5 \times 10^{14}$  ions/cm<sup>2</sup>sec and a fluence of  $10^{17}$  ions/cm<sup>2</sup>.

The etched graphite samples were reexamined with the STM using the same operating parameters and, if possible, the same tunneling tip used prior to sputtering. The results shown in this study were reproducible from sample to sample and even with different tunneling tips, demonstrating that tip imaging artifacts were minimal. Topographs with obvious imaging artifacts were observed, but were discarded. Figures 1–3 show 2400 Å × 2400 Å images of sputtered graphite, etched at the lower flux, for the three different ion fluences. The corresponding correlation functions are shown in Fig. 4(a). The sample aver-

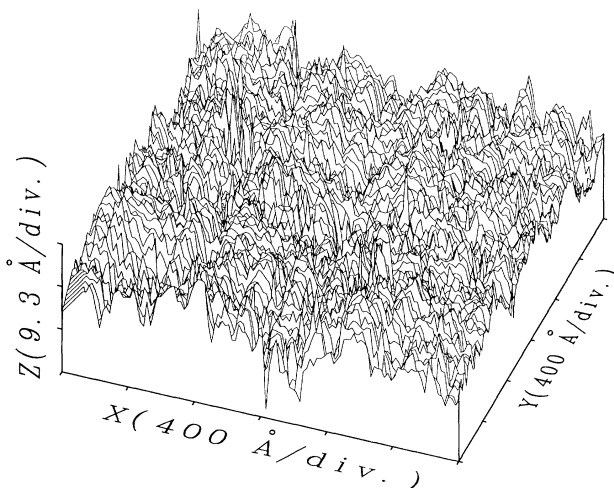


FIG. 2. STM topograph with the same parameters as that in Fig. 1, except that  $Q = 10^{17}$  ions/cm<sup>2</sup> and the total  $Z$  scale is 27.9 Å.

age  $\langle |h(\mathbf{q})|^2 \rangle$  was obtained by summing  $|h(\mathbf{q})|^2$  at each value of  $\mathbf{q}$  for increments of 1° over an angular range of 180°, since by symmetry only half of the Fourier transform was needed. The variance of  $\langle |h(\mathbf{q})|^2 \rangle$  was also calculated to provide an estimate of the uncertainty in the correlation function.

The surface morphology is observed to be a function of the ion fluence in Figs. 1–3 and Fig. 4(a). By comparing Fig. 4(a) to 4(b), which shows the correlation functions for samples sputtered with the same fluences as in Fig. 4(a) but with a 5 times higher flux, one can also see the surprising result that the surface roughness increases strongly with the ion flux, since the numerical values of  $\langle |h(\mathbf{q})|^2 \rangle$  are much larger for the higher flux. A compar-

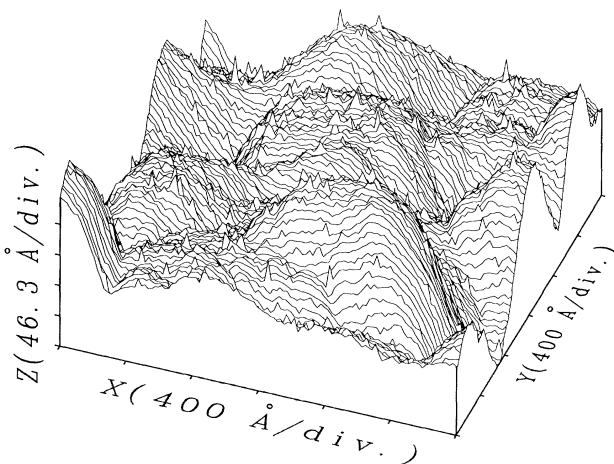


FIG. 3. STM topograph with the same parameters as that in Fig. 1, except that  $Q = 10^{18}$  ions/cm<sup>2</sup> and the total  $Z$  scale is 231.5 Å.

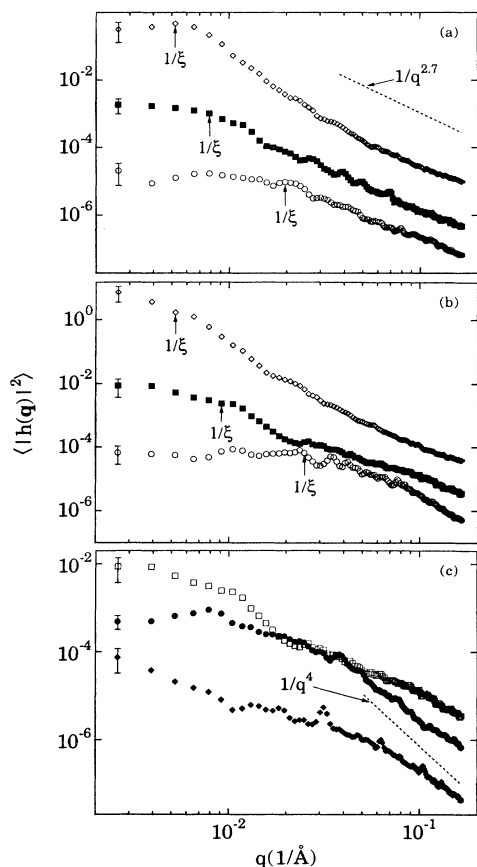


FIG. 4. Height-correlation functions: (a)  $\langle |h(\mathbf{q})|^2 \rangle$  for the data in Figs. 1-3, with  $Q = 10^{16}$  ions/cm<sup>2</sup> (○),  $10^{17}$  ions/cm<sup>2</sup> (■), and  $10^{18}$  ions/cm<sup>2</sup> (◇). The crossover wave vector  $q_0 = 1/\xi$  is indicated for each curve and a  $1/q^{2.7}$  dependence is shown for comparison in the large- $q$  regime. The error bars indicate 1 standard deviation in  $\langle |h(\mathbf{q})|^2 \rangle$ . The uncertainty decreases as  $q$  increases and at large  $q$  the error bars are within the size of the symbols for the data points. (b)  $\langle |h(\mathbf{q})|^2 \rangle$  for topographs with the same parameters as in (a), except that the flux is higher:  $J = 3.5 \times 10^{14}$  ions/cm<sup>2</sup>sec. Note that at this flux, the surfaces are significantly rougher than those represented in (a), i.e.,  $\langle |h(\mathbf{q})|^2 \rangle$  is larger at all values of  $q$ . (c) Temperature dependence of  $\langle |h(\mathbf{q})|^2 \rangle$  with  $J = 3.5 \times 10^{14}$  ions/cm<sup>2</sup>sec,  $Q = 10^{17}$  ions/cm<sup>2</sup>, and  $T = 300$  K (□),  $T = 600$  K (●), and  $T = 900$  K (◆). A  $1/q^4$  dependence is shown for comparison in the large- $q$  regime. Note that  $\langle |h(\mathbf{q})|^2 \rangle$  decreases (the surfaces are smoother) with increasing  $T$ .

ison of the data to the existing theories will help in understanding the observed trends.

If we define the corrugation as the slope of a line connecting two points on a surface, Fig. 1 shows that for low fluence, this quantity becomes small for points separated by lengths larger than the correlation length,  $\xi \approx 100$ – $200$  Å. Thus, for such length scales, the surface can be considered to be flat. As the fluence  $Q$  increases  $\xi$  increases as well, and at the highest fluence  $\xi$  exceeds the image size. For this real-space behavior, one would ex-

pect that the correlation function should be  $q$  independent for  $q \lesssim 1/\xi$ , while it should decrease with  $q$  for  $q \gtrsim 1/\xi$ , as observed in Figs. 4(a) and 4(b).

The creation of correlated structures by particle radiation appears to be counterintuitive. However, theoretical studies of the nonequilibrium growth of interfaces [11,12] show that the formation of correlated structures from a stochastic process is possible. A general scaling description [12] has been developed in the context of various growth models [11]. According to this scaling theory,

$$\langle |h(\mathbf{q})|^2 \rangle_t \propto q^{-\nu} F(tq^z), \quad (2)$$

with  $F(x) \propto x^{\nu/z}$  for small  $x$ , and  $F(x) \sim \text{const}$  for large  $x$ . This would predict a power-law decrease,  $q^{-\nu}$ , in  $\langle |h(\mathbf{q})|^2 \rangle_t$  for  $q \gtrsim t^{-1/z}$ . Under conditions of rotational invariance, the exponent  $z$  is related to  $\nu$  by  $z = 2 - \alpha$ , with  $2\alpha = \nu - 2$ . The values of  $\alpha$  obtained from numerical studies in three dimensions are model dependent [16]. For weak nonlinearity,  $\alpha$  values in the range 0.15–0.23 were reported [16], while  $\alpha$  is  $\sim 0.4$  for strong coupling.

Radiation erosion has so far been modeled only within the context of a *linear-response* theory [17], in which one assumes that

$$\partial_t h(\mathbf{q}, t) = -\omega(\mathbf{q})h(\mathbf{q}, t) + \eta(\mathbf{q}, t), \quad (3)$$

where  $\omega(\mathbf{q})$  is the healing rate of a surface modulation of wave vector  $\mathbf{q}$  and  $\eta(\mathbf{q}, t)$  is the Gaussian white noise for the incident ions with a variance proportional to the flux  $J$ . The corresponding correlation function is

$$\langle |h(\mathbf{q})|^2 \rangle_t \propto \frac{J}{\omega(\mathbf{q})} \{1 - \exp[-\omega(\mathbf{q})t]\}, \quad (4)$$

which predicts that the surface roughness should depend upon the ion flux, as is observed experimentally. For the case of isotropic radiation erosion, which is not strictly valid for our experiments because the sample was etched by an ion beam, and including annealing by both an evaporation-recondensation-like mechanism and surface diffusion, the healing rate is [17]

$$\omega(\mathbf{q}) \propto J|\mathbf{q}| + \gamma|\mathbf{q}|^2 + D|\mathbf{q}|^4, \quad (5)$$

with  $\gamma$  the healing rate for redeposition process and  $D$  proportional to the surface diffusion constant.

By expanding the exponential term in Eq. (4) for the limit  $q \rightarrow 0$ , we see that the interface width,

$$W \equiv \lim_{q \rightarrow 0} \langle |h(\mathbf{q})|^2 \rangle_t^{1/2},$$

should be proportional to  $(Jt)^{1/2} = Q^{1/2}$ , a prediction which is *independent* of the choice of the healing-rate function  $\omega(q)$ . This is just the behavior one expects from a stochastic process, i.e., the removal of material from random locations on the surface by the incident ions. Linear-response theory is, for large  $J$ , a special case of Eq. (2) with  $\nu = z = 1$ .

As a first test of theory, both Eqs. (2) and (4) predict that for small  $q$ ,  $\langle |h(\mathbf{q})|^2 \rangle_t$  is proportional to  $t$  (or  $Q$ ) and

is independent of  $q$ , while for large  $q$  it should decrease with  $q$ , indicating two distinct regions in plots of  $\langle |h(\mathbf{q})|^2 \rangle_t$  vs  $q$ . Figures 4(a) and 4(b) show that this behavior is exactly what is seen experimentally. The crossover occurs at  $q = \xi^{-1}(t)$ . Scaling theory predicts  $\xi(t) \propto t^{1/2}$ , while linear-response theory predicts  $\xi(t) \propto Jt$  [assuming  $\xi q \lesssim (\omega/J)^{1/3}$ ]. From Figs. 4(a) and 4(b), we find that  $\xi$  increases with fluence  $Q = Jt$ , but more slowly than linearly.

As the second test, we examine  $\xi(t)$  in the plots of  $\langle |h(\mathbf{q})|^2 \rangle_t$  in Fig. 4(b). Linear-response theory predicts that  $\xi(t)$  should be independent of flux. Indeed, within the uncertainties of the experimental data,  $\xi$  does not appear to have changed significantly for surfaces sputtered with the higher flux, even though these surfaces were significantly rougher.

Next, for large  $q$  scaling theory predicts a  $q^{-\nu}$  power-law dependence. In Fig. 4(a), we see an approximate power-law dependence in the correlation function at large  $q$  for the lower ion fluences, with an associated exponent  $\nu$  of order 2.5–2.9, so scaling would then predict  $z \sim 1.6$ –1.8. As a consequence,  $\xi(t) \sim t^{1/2}$  should increase slower whereas  $W^2(t) \sim t^{\nu/2}$  should increase faster than linearly with time or fluence. Both of these dependences are observed in the data, so the interface width of the sputter-etched graphite does not have the  $Q^{1/2}$  dependence expected of a simple stochastic process.

Finally, we also investigated the surface morphology at elevated temperatures  $T$ . Since surface diffusion constants rapidly increase with  $T$ , we expect from Eq. (4) that  $\lim_{q \rightarrow \infty} \langle |h(\mathbf{q})|^2 \rangle_t \propto J/Dq^4$  at high temperature. In Fig. 4(c), we show the  $T$  dependence of  $\langle |h(\mathbf{q})|^2 \rangle$  for  $J = 3.5 \times 10^{14}$  ions/cm sec and  $Q = 10^{17}$  ions/cm<sup>2</sup>. Above 600 K,  $\langle |h(\mathbf{q})|^2 \rangle$  drops more sharply with  $q$  and, for large  $q$ , appears to have a  $q^{-4}$  tail. For lower  $T$ , we found no  $q^{-4}$  tail down to  $0.1 \text{ \AA}^{-1}$  in any of our topographs.

In summary, under continued ion bombardment, graphite surfaces evolve toward a rough phase characterized by the divergence of the correlation length. Our data decisively rule out any linear-response treatment as a viable quantitative theory of radiation erosion, although our results are consistent with a number of the qualitative aspects of Eq. (4). Our results are also consistent with the scaling ansatz of Eq. (2), but noise in the data prevents accurate determination of the exponents. Nevertheless, we can rule out the “trivial” case  $\nu = z = 1$ . From our data at lower fluences, we find the exponent  $\alpha$  to lie in the range 0.2–0.4, which appears to be consistent with

the exponents found for the local growth models [16]. We find this agreement somewhat surprising, as there is no *a priori* reason to expect a local growth model to correctly describe erosion via sputtering [17].

This work was supported by the National Science Foundation through Grant No. DMR 8922027 and by the Office of Naval Research. We would like to thank L. Golubovic and R. P. U. Karunasiri for helpful discussions and E. J. Snyder for assistance with the computer software.

- 
- [1] J. L. Vossen and W. Kern, *Thin-Film Processes* (Academic, New York, 1978).
  - [2] H. J. Mathieu, in *Thin Film and Depth Profile Analysis*, edited by H. Oeschner (Springer-Verlag, Berlin, 1984), pp. 39–58.
  - [3] G. Carter, in *Erosion and Growth of Solids Stimulated by Atom and Ion Beams*, edited by G. Kiriakidis, G. Carter, and J. L. Whitton (Martinus Nijhoff, Hingham, MA, 1986), pp. 70–97.
  - [4] I. J. Hodginson and P. W. Wilson, *CRC Rev.* **15**, 27 (1988).
  - [5] See, for example, G. Carter and M. J. Nobes, *Earth Surf. Processes* **5**, 131 (1980).
  - [6] I. V. Katardjiev, *J. Vac. Sci. Technol. A* **6**, 2434 (1988).
  - [7] J. A. Kubby and B. M. Siegel, in *Erosion and Growth of Solids Stimulated by Atom and Ion Beams* (Ref. [3]), pp. 444–452.
  - [8] See, for example, D. M. Mattox, *J. Vac. Sci. Technol. A* **7**, 1105 (1989).
  - [9] G. Carter, B. Navinsek, and J. L. Whitton, in *Sputtering by Particle Bombardment*, edited by R. Behrisch (Springer-Verlag, Berlin, 1983), Vol. II, pp. 231–266.
  - [10] G. K. Wehner, *J. Vac. Sci. Technol. A* **3**, 1821 (1985).
  - [11] M. Kardar, G. Parisi, and Y. C. Zhang, *Phys. Rev. Lett.* **56**, 889 (1986). For a review, see T. Vicsek, *Fractal Growth Phenomena* (World Scientific, Singapore, 1989).
  - [12] F. Family and T. Vicsek, *J. Phys. A* **18**, L75 (1985).
  - [13] P. K. Hansma and J. Tersoff, *J. Appl. Phys.* **61**, R1 (1987).
  - [14] For earlier measurements of  $\langle |h(\mathbf{q})|^2 \rangle$  by microscopy, see G. Rasigni *et al.*, *Surf. Sci.* **162**, 985 (1985).
  - [15] J. D. Weeks, *Ordering in Strongly Fluctuating Condensed Matter Systems* (Plenum, New York, 1980), p. 293.
  - [16] H. Yan, D. Kessler, and L. M. Sander, *Phys. Rev. Lett.* **64**, 926 (1990).
  - [17] G. S. Bales, R. Bruinsma, E. A. Eklund, R. P. U. Karunasiri, J. Rudnick, and A. Zangwill, *Science* **249**, 264 (1990).